Costameric integrin and sarcoglycan protein levels are altered in a *Drosophila* model for Limb-girdle muscular dystrophy type 2H

Simranjot Bawa[a], Samantha Gameros[a], Kenny Baumann[b], David S. Brooks[a], Joseph A. Kollhoff[a], Michal Zolkiewski[a], Andrea David Re Cecconi[c], Nicolò Panini[d], Massimo Russo[d], Rosanna Piccirillo[c], David K. Johnson[e], Maithri M. Kashipathy[f], Kevin P. Battaile[g], Scott Lovell[f], Samuel E.A. Bouyain[b], Jessica Kawakami[b], and Erika R. Geisbrecht[a,b,*]

[a]Department of Biochemistry and Molecular Biophysics, Kansas State University, Manhattan, KS 66506; [b]School of Biological Sciences, University of Missouri—Kansas City, MO 64110; [c]Department of Neuroscience and [d]Department of Oncology, Istituto di Ricerche Farmacologiche Mario Negri IRCCS, 20156 Milan, Italy; [e]Molecular Graphics and Modeling Laboratory, Computational Chemical Biology Core, and [f]Protein Structure Laboratory, University of Kansas, Lawrence, KS 66047; [g]NYX, New York Structural Biology Center, Upton, NY 11973

ABSTRACT **Mutations in two different domains of the ubiquitously expressed TRIM32 protein give rise to two clinically separate diseases, one of which is Limb-girdle muscular dystrophy type 2H (LGMD2H). Uncovering the muscle-specific role of TRIM32 in LGMD2H pathogenesis has proven difficult, as neurogenic phenotypes, independent of LGMD2H pathology, are present in *TRIM32 KO* mice. We previously established a platform to study LGMD2H pathogenesis using *Drosophila melanogaster* as a model. Here we show that LGMD2H disease-causing mutations in the NHL domain are molecularly and structurally conserved between fly and human TRIM32. Furthermore, transgenic expression of a subset of myopathic alleles (R394H, D487N, and 520fs) induce myofibril abnormalities, altered nuclear morphology, and reduced TRIM32 protein levels, mimicking phenotypes in patients afflicted with LGMD2H. Intriguingly, we also report for the first time that the protein levels of βPS integrin and sarcoglycan δ, both core components of costameres, are elevated in TRIM32 disease-causing alleles. Similarly, murine myoblasts overexpressing a catalytically inactive TRIM32 mutant aberrantly accumulate α- and β-dystroglycan and α-sarcoglycan. We speculate that the stoichiometric loss of costamere components disrupts costamere complexes to promote muscle degeneration.**

Monitoring Editor
Alpha Yap
University of Queensland

Received: Jul 13, 2020
Revised: Nov 12, 2020
Accepted: Nov 25, 2020

INTRODUCTION

Limb-girdle muscular dystrophy (LGMD) represents a group of genetically inherited disorders characterized by progressive muscle degeneration that initially affects proximal limb muscles (Guglieri *et al.*, 2008; Mahmood and Jiang, 2014). Clinical examination and muscle biopsies of LGMD patients reveal heterogeneity in disease onset, with patients experiencing mild to severe muscle damage, making treatment options difficult. The majority of mutated genes that result in over 31 subtypes of LGMD encode for muscle structural proteins (Murphy and Straub, 2015; Tocchini and Ciosk, 2015). In contrast, patients diagnosed with LGMD2H have mutations in the E3 ubiquitin ligase TRIM32. The N-terminus of TRIM32 is characterized by a Really Interesting New Gene (RING) domain, B-box domain, and coiled-coil region, followed by six Ncl-1, HT2A, Lin-41 (NHL) repeats in the C-terminus (Sardiello *et al.*, 2008; Tocchini and Ciosk, 2015). A mutation in the B-box region gives rise to Bardet–Biedl syndrome (BBS), a disease whose clinical presentation shares no muscle pathology. The pathogenic mechanism associated with BBS is not fully understood (Chiang *et al.*, 2006).

The LGMD2H causative mutation c.1459G>A (p.D487N) in *TRIM32* was first identified in Manitoba Hutterite descendants in

This article was published online ahead of print in MBoC in Press (http://www.molbiolcell.org/cgi/doi/10.1091/mbc.E20-07-0453) on December 9, 2020.

*Address correspondence to: Erika R. Geisbrecht (geisbrechte@ksu.edu).

Abbreviations used: DGC, dystrophin–glycoprotein components; LGMD2H, Limb-girdle muscular dystrophy type 2H; L3, third instar larvae; REU, Rosetta energy units; Scgδ, sarcoglycan δ; TM, tropomyosin.

North America (Shokeir and Kobrinsky, 1976; Frosk *et al.*, 2002, 2005). Subsequently, the same mutation was also reported in patients with sarcotubular myopathy (STM), suggesting that STM and LGMD2H are allelic disorders, with vacuolar pathology more prominent in STM (Frosk *et al.*, 2005; Schoser *et al.*, 2005). More recently, one reported mutation in the RING domain and additional mutations in the NHL repeats of TRIM32 have been documented in patients of non-Hutterite origins. Some of these mutations result in partial or complete deletions of the gene, further complicating the analysis (Servián-Morilla *et al.*, 2019). Common characteristics of LGMD2H/STM include rounded muscle fibers with increased internalized nuclei and degenerative/atrophic myofibers, followed by Z-line streaming with a dilated and vacuolated sarcotubular system (Frosk *et al.*, 2005; Schoser *et al.*, 2005; Kudryashova *et al.*, 2009; Servián-Morilla *et al.*, 2019).

TRIM32 localizes to the Z-disk in both mammalian and *Drosophila* skeletal muscle, suggesting a major function in maintaining sarcomeric structure and physiology (Locke *et al.*, 2009; LaBeau-DiMenna *et al.*, 2012; Domsch *et al.*, 2013). Numerous muscle proteins such as actin, desmin, dysbindin, and tropomyosin have been identified as substrates of TRIM32 E3 ligase activity (Locke *et al.*, 2009; Cohen *et al.*, 2012). While the abnormal accumulation of sarcomeric proteins has been reported in various myopathies (Fielitz *et al.*, 2007), the relationship between altered myoprotein levels and/or localization and muscle degeneration remains elusive in LGMD2H disease progression. In healthy muscle tissue, the ubiquitin proteasome system (UPS) is a pivotal component of protein quality control that regulates muscle protein turnover and preserves proteolytic homeostasis (Ciechanover, 2006). Proteins destined for proteasomal degradation are covalently attached by K48-linked polyubiquitin molecules (Thrower *et al.*, 2000). This ubiquitination reaction requires functional cooperation between E1 (ubiquitin-activating enzyme), E2 (ubiquitin-conjugating enzyme), and E3 (ubiquitin ligase) proteins (Weissman, 2001). The RING domain in TRIM E3 ligases confers the enzymatic activity to transfer ubiquitin molecules onto target proteins to specify their fate and/or function (Metzger *et al.*, 2014). The C-terminal NHL domain is implicated in mediating protein–protein interactions and in the recognition of substrates for E3 ligase activity (Tocchini and Ciosk, 2015). Therefore, we predict that the mutations that cluster in the TRIM32_NHL repeats could directly affect the ubiquitination and/or localization of substrate proteins, thereby exacerbating muscle degeneration. Hence, it is critical to study the dual coordination between the RING and NHL domains to improve our understanding of protein stability and function.

The generation of *TRIM32KO* knockout (KO) mice was a key advance in the muscular dystrophy field (Kudryashova *et al.*, 2009). However, the presence of both neurogenic and myopathic defects in *TRIM32KO* mice has increased the difficulty of uncovering the muscle-specific role of TRIM32 in LGMD2H pathogenesis. Two current models, which are not mutually exclusive, postulate roles for TRIM32 in LGMD2H disease progression. Strong evidence supports a model in which TRIM32-deficient satellite cells contribute to disease pathogenesis. TRIM32 is up-regulated in proliferating satellite cells and loss of this protein prevents myotube regeneration (Kudryashova *et al.*, 2012; Nicklas *et al.*, 2012; Assereto *et al.*, 2016). Second, the deregulation of muscle substrates, including actin, α-actinin, tropomyosin, and desmin, may influence muscle degeneration (Cohen *et al.*, 2012). Data support a role for TRIM32 in mediating levels of these proteins in muscle atrophy, but studies have not been performed to directly test this model in the context of LGMD2H. Thus, understanding additional targets of TRIM32-mediated protein regulation may uncover additional mechanisms of TRIM32 pathogenesis.

The progressive muscle degeneration and weakness associated with myopathies and muscular dystrophies are often a result of compromised mechanical stability in the myofiber costameric apparatus (Jaka *et al.*, 2015). The dystrophin–glycoprotein components (DGC), along with the sarcoglycan subcomplex (α, β, γ, δ, ε, and ζ) and the integrin–vinculin–talin network, form costameric complexes at the sarcolemma and Z-disk that are essential to the integrity of skeletal muscle (Henderson *et al.*, 2017). The sarcoglycan transmembrane glycoproteins are predominantly expressed in striated muscle and form subcomplexes with sarcospan to provide DGC stability at the membrane (Campbell and Kahl, 1989; Ervasti *et al.*, 1990; Crosbie *et al.*, 1999). Mutations that affect sarcoglycan proteins α, β, γ, and δ are implicated in autosomal recessive LGMD types 2 C–F (Nigro and Savarese, 2014). Similarly to the sarcoglycans, integrins are also transmembrane cell surface receptors and mediate the interaction between the actin cytoskeleton and extracellular matrix (ECM) proteins. Integrin heterodimers are composed of α and β subunits, and this assembly is essential for ligand binding and signal transduction (Hynes, 2004; Barczyk *et al.*, 2010). Integrin complex function is broadly required in skeletal muscle for myogenic cell differentiation, migration, sarcomerogenesis, and satellite cell regeneration (Vachon *et al.*, 1997; Liu *et al.*, 2011). Mice deficient in α_7 integrin in muscle exhibit altered muscle fiber morphology and are susceptible to exercise-induced injury (Hayashi *et al.*, 1998; Schwander *et al.*, 2003; Boppart and Mahmassani, 2019).

We previously reported that loss of *Drosophila thin (tn),* which encodes for TRIM32, compromises the integrity of integrin-associated complexes (LaBeau-DiMenna *et al.*, 2012). Here we take advantage of innate features in the *Drosophila* LGMD2H model to determine how LGMD2H pathological alleles (R394H, D487N, and 520fs) contribute to disease progression. The lack of stem cells in *Drosophila* larval muscle presents an opportunity to observe disease progression without the complications of differentiation and repair (Piccirillo *et al.*, 2014). Moreover, the absence of an adaptive immune system in flies prevents the infiltration of cell types that promote inflammation and disease progression in mammalian muscular dystrophies. Here we show that the myogenic expression of human disease alleles results in *Drosophila* muscle degeneration, reduced TRIM32 protein levels, and the abnormal accumulation of βPS integrin and Scgδ. Extending these findings in mammals, the levels of costamere proteins such as α- and β-dystroglycans and α-sarcoglycan are elevated in catalytically defective TRIM32-expressing murine cells, suggesting that costamere complex integrity is essential to prevent LGMD2H disease progression.

RESULTS

Loss of *Drosophila tn* is a muscle-specific model for LGMD2H

We and others previously showed that the progressive muscle degeneration in *tn* mutants (*tn–/–*) is initiated after embryogenesis and is concurrent with increased larval muscle activity (LaBeau-DiMenna *et al.*, 2012). This loss of muscle integrity is particularly apparent in the skeletal or body wall muscles of third instar larvae (L3) stained with phalloidin to label F-actin. *Wild-type* (*WT)* L3 muscles revealed a striated pattern of sarcomeres (Figure 1, A and A′), in which *tn–/–* muscles were thinner, with a loss of structural integrity (Figure 1, B and B′). Because *TRIMKO* mice exhibit both neurological and myopathic phenotypes that may contribute to altered muscle morphology (Kudryashova *et al.*, 2009), we directly examined which tissue contributes to muscle degeneration in our *Drosophila* model by reducing TRIM32 function in either muscles or neurons using the Gal4/UAS system. Consistent with previous

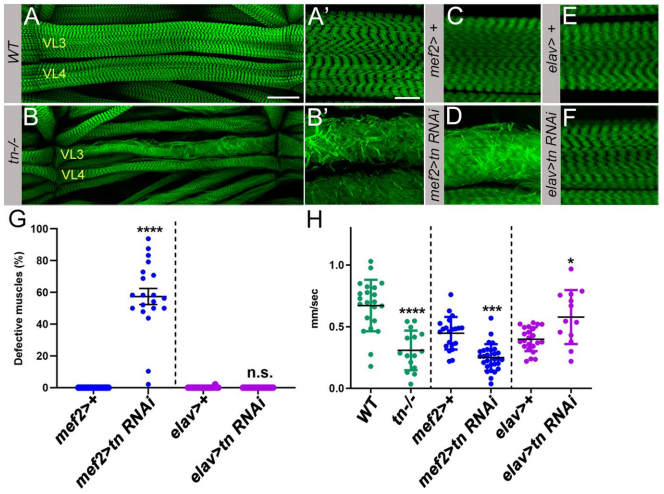

FIGURE 1: Muscle degeneration is neuron-independent. (A, B) L3 larval ventral longitudinal muscles 3 (VL3) and 4 (VL4) stained with phalloidin to visualize F-actin (green). (A, A') The stereotypical morphology of *WT* muscle with normal sarcomeric organization. (B, B') In addition to sarcomeric disorganization, the VL3 and VL4 muscles are noticeably smaller in *tn–/–* larvae. (C–F) Phalloidin labeling of VL3 muscles in L3 larvae. Muscle morphology is unaffected in *mef2*-Gal4, C, or *elav*-Gal4, E, driver controls. Dystrophic muscle is apparent upon muscle-specific *tn RNAi*, D, but not upon a decrease of TRIM32 in neurons, F. (G) Quantification shows that induction of *tn RNAi* in muscles, but not neurons, results in muscle defects. (H) Locomotion assay performed on L3 larvae shows a decrease in mobility upon loss of TRIM32 (*tn–/–*) or the induction of *tn RNAi* in muscle tissue (*mef2>tn RNAi*). The reduction in locomotion is minor upon neuronal-specific RNAi knockdown of TRIM32 (*elav>tn RNAi*). Mean ± SEM. ****, $p < 0.001$; *, $p < 0.05$; n.s., not significant. Scale bars: 50 µm, A, B; 25 µm, A', B', C–F.

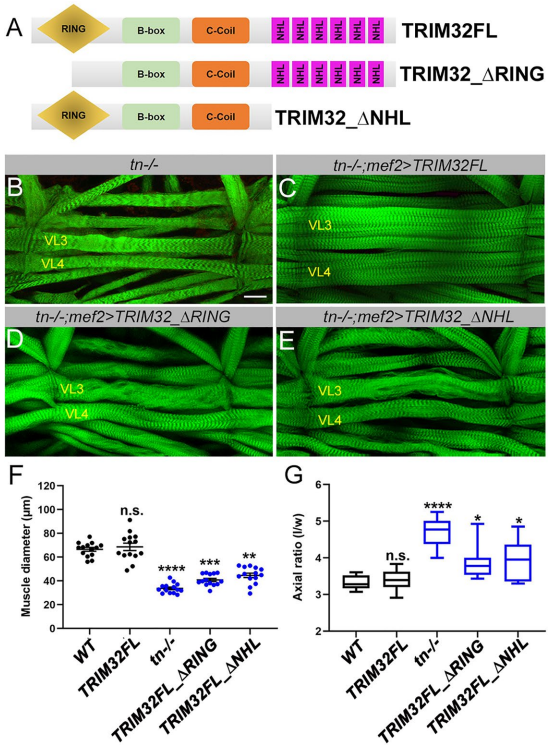

FIGURE 2: RING and NHL domain deletion mutants limit muscle growth and induce degeneration. (A) Schematic representation of the RING, B-box, coiled-coil, and NHL domains in TRIM32FL and the TRIM32 deletion mutants. (B–E) VL3 and VL4 muscles stained for F-actin to visualize muscle fiber structure in L3 larvae. (B) *tn–/–* mutant muscles appear thinner with prominent sarcomere patterning defects. (C) Overexpression of TRIM32FL under control of the *mef2* promoter in a *tn–/–* background (*tn–/–; mef2*>TRIM32FL) rescued muscle morphology defects. (D, E) Deletion of either the RING, D, or the NHL domain, E, mimics the loss of *TRIM32* function phenotype. In addition to muscle morphology defects, Δ*RING* and Δ*NHL* deletion mutants exhibited noticeably thinner VL3 and VL4 muscles similar to *tn* mutants. (F) A scatterplot showing VL3 muscle diameter in the indicated genotypes. Note that *TRIM32FL, TRIM32_ΔRING,* and *TRIM32_ΔNHL* are all expressed in a *tn–/–* background. Deletion of RING or NHL domains reduces VL3 muscle diameter, while muscle expression of *TRIM32FL* rescues this muscle loss. (G) Box and whisker plot of the pupal case axial ratios show Δ*RING* and Δ*NHL* deletion mutants are defective in muscle contraction, although not quite as severe as *tn* mutants. Note that *TRIM32FL, TRIM32_ΔRING,* and *TRIM32_ΔNHL* are all expressed in a *tn–/–* background. Mean ± SEM. ****, $p < 0.001$; ***, $p < 0.005$; **, $p < 0.01$; *, $p < 0.05$; n.s., not significant. Scale bars: 50 µm, B–E.

results (LaBeau-DiMenna *et al.*, 2012), the structural deficits associated with muscle-specific RNAi knockdown of TRIM32 (*mef2>tn RNAi*; Figure 1, C, D, and G) also reduced the locomotor ability of L3 larvae in a way comparable to that in *tn–/–* larvae (Figure 1H). However, this same reduction of TRIM32 under control of a pan-neuronal promoter (*elav>tn RNAi*) did not alter muscle structure (Figure 1, E–G) or function (Figure 1H). These results further support published data whereby the reintroduction of TRIM32 solely into muscle tissue rescues the *tn–/–* dystrophic muscle phenotype (LaBeau-DiMenna *et al.*, 2012; Domsch *et al.*, 2013; Bawa *et al.*, 2020). Importantly, our *Drosophila* LGMD2H model can be used to assess the muscle-specific function of TRIM32, thus avoiding neurogenic phenotypes present in *TRIM32KO* mice that may contribute indirectly to disease pathology.

The RING domain and NHL repeats are indispensable for TRIM32 function

In addition to muscle degeneration, a unique feature of *tn–/–* muscles is a notable reduction in muscle size. We recently uncovered a mechanistic link between muscle growth and metabolism, in which a loss of TRIM32 causes thinner muscles, due to defects in the glycolytically driven accumulation of biomass (Bawa *et al.*, 2020). Therefore, to explore the role of the RING or NHL domains in promoting muscle growth, we generated and analyzed transgenic flies expressing UAS-based *TRIM32FL*, *TRIM32_ΔRING*, or *TRIM32_ΔNHL* constructs (Figure 2A) under control of the *mef2* promoter in a *tn–/–* background (Figure 2B). As expected, expression of full-length TRIM32 in muscle tissue rescued the TRIM32-associated myofibrillar anomalies and muscle size defects (Figure 2, C and F). Consistent with results reported by the Nguyen lab (Domsch *et al.*, 2013), L3 muscle expression of TRIM32 devoid of either the RING domain (Figure 2D) or NHL repeats (Figure 2E) showed muscle degeneration similar to that in *tn* mutants. Quantification of the ventral longitudinal 3 (VL3) muscle diameter of both the *TRIM32_ΔRING* and *TRIM32_ΔNHL* deletions in a *tn–/–* background showed considerably reduced muscle size as compared with the *TRIM32FL* rescue animals (Figure 2F). Taken together, our observations provide evidence that loss of either the RING domain or NHL repeats causes constraints in metabolic machinery, resulting in smaller muscles.

We next investigated the functional consequences of the abnormal muscle morphology present in the *TRIM32_ΔRING* and

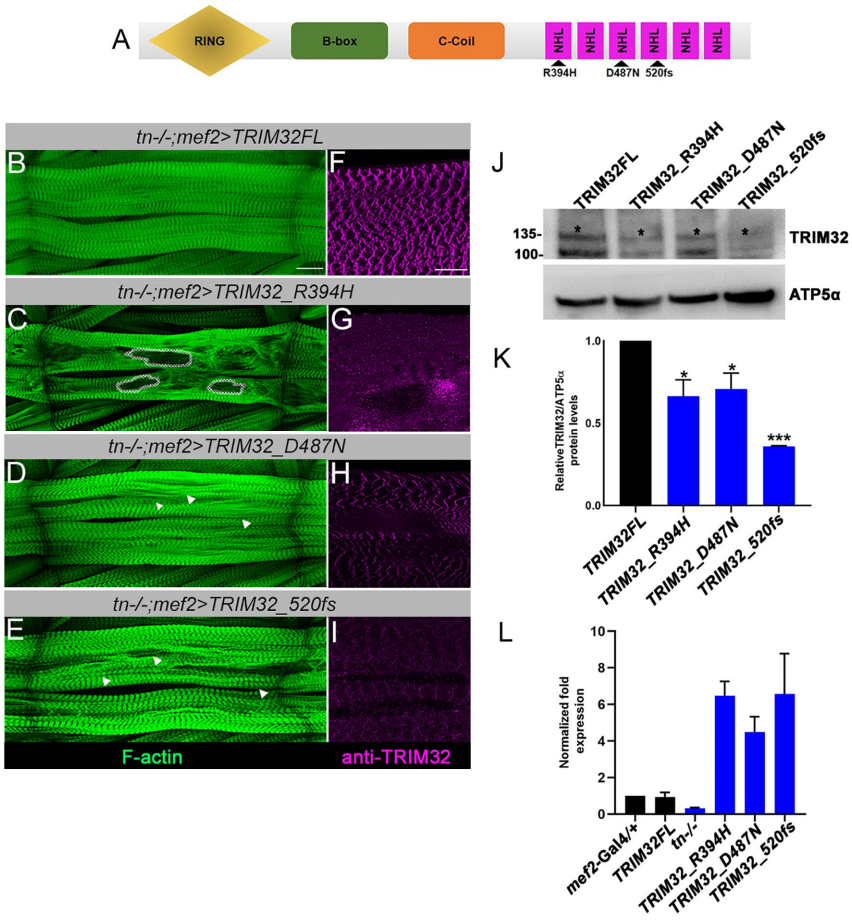

FIGURE 3: Expression of LGMD2H disease-causing alleles causes dystrophic muscle and reduces TRIM32 protein levels. (A) Relative location of human TRIM32 mutations in NHL1 (R394H), NHL3 (D487N), or NHL4 (fs520). (B–E) Phalloidin-labeled body wall muscles in L3 larvae. (B) *TRIM32FL* control animals (*tn-/-;mef2>TRIM32FL*) show *WT* muscle morphology. (C–E) Expression of human pathogenic mutations in a *tn* mutant background cause defects in muscle morphology. (C) Muscle expression of the *R394H* mutation (*tn–/–;mef2>TRIM32_R394H*) resulted in extensive muscle damage. Dotted lines indicate absence of sarcomeric structure. (D, E) The severity of the *D487N*, D, or *520fs*, E, mutations in larval musculature was milder than that of *R394H* mutant muscles, C, with myofibrillar abnormalities represented by white arrowheads. (F–I) TRIM32 protein localization in L3 muscle tissue upon transgene expression in a *tn–/–* background. (F) Z-disk expression of TRIM32 in *tn–/–; mef2>TRIM32FL* muscle. (G–I) Z-disk localization appears normal, yet is reduced in protein amounts upon expression of pathogenic alleles. (J) Western blot analysis of whole larvae shows decreased TRIM32 protein levels in *R394H, D487N* or *520fs* mutants compared with *TRIM32FL* controls. ATP5α is used as a loading control. (K) Bar graph depicts the relative intensity of TRIM32 protein levels normalized to ATP5α in the indicated genotypes. $N = 3$. (L) qPCR reveals that *tn* transcripts are indeed present in muscle carcasses upon expression of all transgenes, with mutant transgenes increased over control (*mef2/+*) or I. mRNA was normalized to *rp49* transcripts. $N = 3$ biological replicates and 3 technical replicates for each genotype. Mean ± SEM. ***, $p < 0.005$; *, $p < 0.05$). Scale bars: 50 μm, A–D; 25 μm, E–H.

TRIM32_ΔNHL deletion mutants. During fly metamorphosis, the transition from the larval to the pupal stages requires body wall muscles to contract. However, failure of this contraction results in an extended pupal case, serving as a proxy for muscle function (LaBeau-DiMenna *et al.*, 2012; Bawa *et al.*, 2020; Brooks *et al.*, 2020). Quantitation of this pupal axial ratio (length/width measurements) was ~3 in *WT* individuals with a median of >4 in *tn–/–* pupae that fail to contract (Figure 2G). Restoration of normal pupal size was obtained after rescue by muscle-expressed *TRIM32FL*. In contrast, both TRIM32 deletion mutants, when expressed in a *tn–/–* background, showed an axial ratio greater ~ 4, indicating defects in muscle contraction (Figure 2). Here we conclude that both RING domain and NHL repeats function together in promoting muscle growth and maintaining normal muscle function.

Human disease-causing mutations result in muscle degeneration and altered nuclear morphology

The identification of pathological mutations that cluster in the NHL repeats implies an essential role for this region in disease progression and, more fundamentally, in TRIM32 function. Therefore, to understand the structural properties of the NHL repeats at the molecular level, we solved the structure of the C-terminal *Drosophila* TRIM32_NHL (dTRIM32_NHL) domain at an improved resolution (1.3 Å) using molecular replacement based upon our previously published structure of dTRIM32_NHL (PDB code 6D69; Bawa *et al.*, 2020). We found that the two structures are nearly identical (Supplemental Figure S1, A and B), featuring a six-bladed β propeller, where each NHL repeat consists of four strands of antiparallel β sheets arranged toroidally around a central axis. Superposition yielded an RMSD deviation of 0.51 Å between Cα atoms (288 residue; Supplemental Table S1). In an effort to model the equivalent human TRIM32_NHL (hTRIM32_NHL) region, a three-dimensional model was obtained using the I-TASSER server. A high degree of similarity was predicted between these two structures despite the modest primary sequence homology (Supplemental Figure S1, C and D). In addition, we observed that the location and conformation of the disease-causing amino acids R394H (*Drosophila* residue R1114) and D487H (*Drosophila* residue D1212) are conserved between the human and fly proteins and may be accessible to mediate intermolecular contacts with the other proteins (Supplemental Figure S1, E and F). Taking these together, our approach provides strong evidence for structural and functional similarities between human and fly TRIM32, making our fly model well suited for studying molecular and cellular properties of human mutations associated with LGMD2H.

The pathological alleles present in the NHL domains of LGMD2H patients vary in origin, consisting of point mutations (R394H, D487N), a single amino acid deletion (D588Δ), frameshift deletions (A422fs, T520fs, L535fs, I590fs) and a stop codon (R613*; Slack and Ruvkun, 1998; Frosk *et al.*, 2002; Saccone *et al.*, 2008; Borg *et al.*, 2009; Cossée *et al.*, 2009). Because the molecular location of the two point mutations is identical between the human and fly TRIM32 proteins, we assessed the cellular impact of these mutations and an additional frameshift mutation in mimicking LGMD2H pathology in the *Drosophila* musculature (Figure 3A). To this end, we once again created transgenic *Drosophila* stocks that recapitulate the *TRIM32_R394H*, *TRIM32_D487N*, and *TRIM32_520fs* myopathic mutations. Each of these pathological alleles was

recombined into a *tn–/–* background and the resulting UAS-based proteins were expressed in muscle using *mef2*-Gal4 for the analysis of L3 larval muscle morphology. As expected, expression of *TRIM32FL* rescued the pupal lethality and reverted the muscle morphology defects present in *tn* mutants back to *WT* (Figure 3B). Independent expression of the *TRIM32_R394H* (Figure 3C), *TRIM32_D487N* (Figure 3D), or *TRIM32_520fs* (Figure 3E) alleles showed substantial, although differential, muscle degeneration. Notably, the phenotypes of *TRIM32_D487N* and *TRIM32_520fs* appeared weaker than a complete loss of TRIM32 (Figure 2B), suggesting that there is partial protein function in the pathogenic alleles. The dominant overexpression of *TRIM32FL*, *TRIM32_D487N*, and *TRIM32_520fs* in a *WT* background did not affect muscle morphology (Supplemental Figure S2, A–C and E). However, overexpression of *TRIM32_R394H* alone displayed myofibril defects (Supplemental Figure S2D), suggesting that the R394H mutation can function in a dominant manner in approximately 50% of the muscles examined (Supplemental Figure S2E). Interestingly, and consistent with this observation, one patient diagnosed with LGMD2H is heterozygous for *R394H/+* mutation (Saccone *et al.*, 2008).

Next, we sought to determine the localization pattern of TRIM32 protein in the larval musculature of each mutant genotype. TRIM32 accumulated at the Z-disk in *TRIM32FL* muscles (Figure 3F). Reduced TRIM32 expression levels were observed in *tn–/–, mef2>TRIM32_R394H* (Figure 3G), *tn–/–, mef2>TRIM32_D487N* (Figure 3H), and *tn–/–, mef2>TRIM32_520fs* (Figure 3I) muscles. To determine if changes in TRIM32 protein levels are concomitant with muscle degeneration in our fly model, we homogenized larvae for each of the myopathic mutants and investigated total protein levels. Western blot analysis showed comparatively reduced TRIM32 protein levels in all mutant alleles compared with *TRIM32FL* controls (Figure 3, J and K). Strikingly, muscle biopsies from LGMD2H patients also showed a severe reduction in TRIM32 protein levels (Servián-Morilla *et al.*, 2019), confirming that our *Drosophila* disease-causing alleles share specific pathophysiological characteristics with LGMD2H patients. To ensure that our transgenes indeed show comparable expression of *TRIM32*-expressing transcripts, we measured mRNA levels via qPCR (Figure 3L). We found that the levels of *TRIM32 mRNA* transcripts were comparable in control (*mef2-Gal4/+*) or *TRIM32FL* rescue carcasses compared with *tn–/–* alone. Interestingly, mRNA levels of all *TRIM32* mutations showed a fourfold to sixfold increase, suggesting that transcript levels are increased to compensate for reduced protein content.

Skeletal muscle fibers are multinucleated and the maintenance of myonuclear structure is essential for regulating the biomechanical properties of muscle tissue (Folker and Baylies, 2013). Multiple nuclear envelope proteins are linked to cytoskeletal elements to mediate stress due to the mechanical forces transmitted during muscle contraction and relaxation. Disturbances in nucleo–cytoskeletal coupling in diseased muscles are often associated with nuclei clustering, irregular spacing, and morphological changes (Skinner and Johnson, 2017). Lamins are structural components of the nuclear lamina that line the inner surface of the nuclear membrane. We recently identified proteins that interact physically with the NHL regions of TRIM32, using an unbiased proteomics approach (Bawa *et al.*, 2020). Interestingly, in these data, there was also an enrichment of nuclear envelope proteins, including *Drosophila* Lamin Dm_o/lamin B-type, Lamin C/lamin A-type, and Barrier to autointegration factor (BAF; Supplemental Table S2). Therefore, to examine if nuclear defects are prominent in our disease-causing alleles, we dissected L3 larvae and immunostained with Lamin to visualize nuclear morphology in VL3 muscles. Myonuclei were flat and oval in *WT* (Supplemental Figure S3A), *tn–/–* (Supplemental Figure S3B), and *tn–/–; mef>TRIM32FL* (Supplemental Figure S3C) larval muscles. However, muscle expression of *TRIM32_R394H* (Supplemental Figure S3D), *TRIM32_D487N* (Supplemental Figure S3E), or *TRIM32_520fs* (Supplemental Figure S3F) in *tn* mutant muscles caused the nuclei to adopt a deformed, elongated shape with a majority of the myonuclei internalized within the myofiber and possessing a nuclear aspect ratio greater than 2 (Supplemental Figure S3G). Moreover, the spacing between nuclei, quantitated as the internuclear distance, was altered in *tn* mutants and the *TRIM32* alleles, with the primary defect being aberrant nuclei clustering (Supplemental Figure S3H). Collectively, the abnormal nuclear architecture in muscles expressing mutated TRIM32 proteins may result from differential interactions with nuclear envelope proteins.

LGMD2H disease-causing alleles leads to adult muscle degeneration

Loss of TRIM32 in multiple *tn* allelic combinations or upon muscle-specific *tn RNAi* is pupal lethal (LaBeau-DiMenna *et al.*, 2012; Domsch *et al.*, 2013; Bawa *et al.*, 2020). Despite the dystrophic changes observed in larval muscle upon expression of our TRIM32 disease-causing mutations, these animals surprisingly survived to adulthood. Therefore, we were able to monitor the impact of aging on muscle structure and disease progression in the adult *Drosophila* indirect flight muscles (IFMs). The IFMs from adult flies were stained with phalloidin and TRIM32 antisera to analyze sarcomere structure and muscle morphology at days 1 through 9 posteclosion. Similarly to *TRIM32FL* control flies (Figure 4, $A_{1\text{-}3}$), adult flies expressing the *TRIM32_D487N* mutation exhibited normal sarcomeric structure at days 1, 3, and 6 (Figure 4, $B_{1–3}$). However, defects due to the D487N mutation became more pronounced by day 9 (Figure $4B_4$). In contrast, the *TRIM32_R394H* and *TRIM32_520fs* mutants displayed profound effects on myofibrillar arrangement starting at day 1 (Figure 4, C_1 and D_1). These structural defects worsened by day 3 (Figure 4, C_2 and D_2) and individual fibers appeared fragmented and were no longer ordered in parallel by days 6 and 9 (Figure 4, $C_{3–4}$ and $D_{3–4}$). Dominant expression of *TRIM32FL* or *TRIM32_D487N* in a *WT* background resulted in IFMs with a normal myofibrillar arrangement (Supplemental Figure S4, A and B), while the dominant effect of *R394H* could not be analyzed, since these individuals died during pupation. However, overexpression of the *TRIM32_520fs* mutation alone caused extensive damage to the myofibers (Supplemental Figure S4C). This latter result is somewhat surprising, since the *TRIM32_fs520* mutation showed a normal phenotype in larval muscle. Nonetheless, these data together suggest that the muscle degeneration in mutant flies is age-dependent.

To further examine the relationship between IFM degeneration, we assessed TRIM32 expression and/or localization in each mutant genotype. TRIM32 localized to the Z-disk and M-line in the adult myofibers of TRIM32FL flies through day 9 (Figure $4A_{1'–4'}$). In *tn–/–; mef2>TRIM32_D487N* mutants, TRIM32 remained localized to the sarcomeres by days 1 and to a much lesser extent by day 3, however protein levels appeared reduced through day 9 (Figure $4B_{1'–4'}$). However, in *tn–/–; mef2>TRIM32_R394H* and *tn–/–; mef2> TRIM32_520fs* mutants, the sarcomeric structure lost integrity at day 1 and TRIM32 appeared diffuse along the degenerative myofibers, with reduced expression through day 9 (Figure 4, $C_{1–4'}$ and $D_{1–4'}$).

We next tested the functional consequences of *TRIM32* disease mutations on flight ability. The total flight distance traveled by individual flies before landing was measured at days 1 and 12 after eclosion. Control (*mef2-Gal4/+*) and *TRIMFL* rescue flies retained the

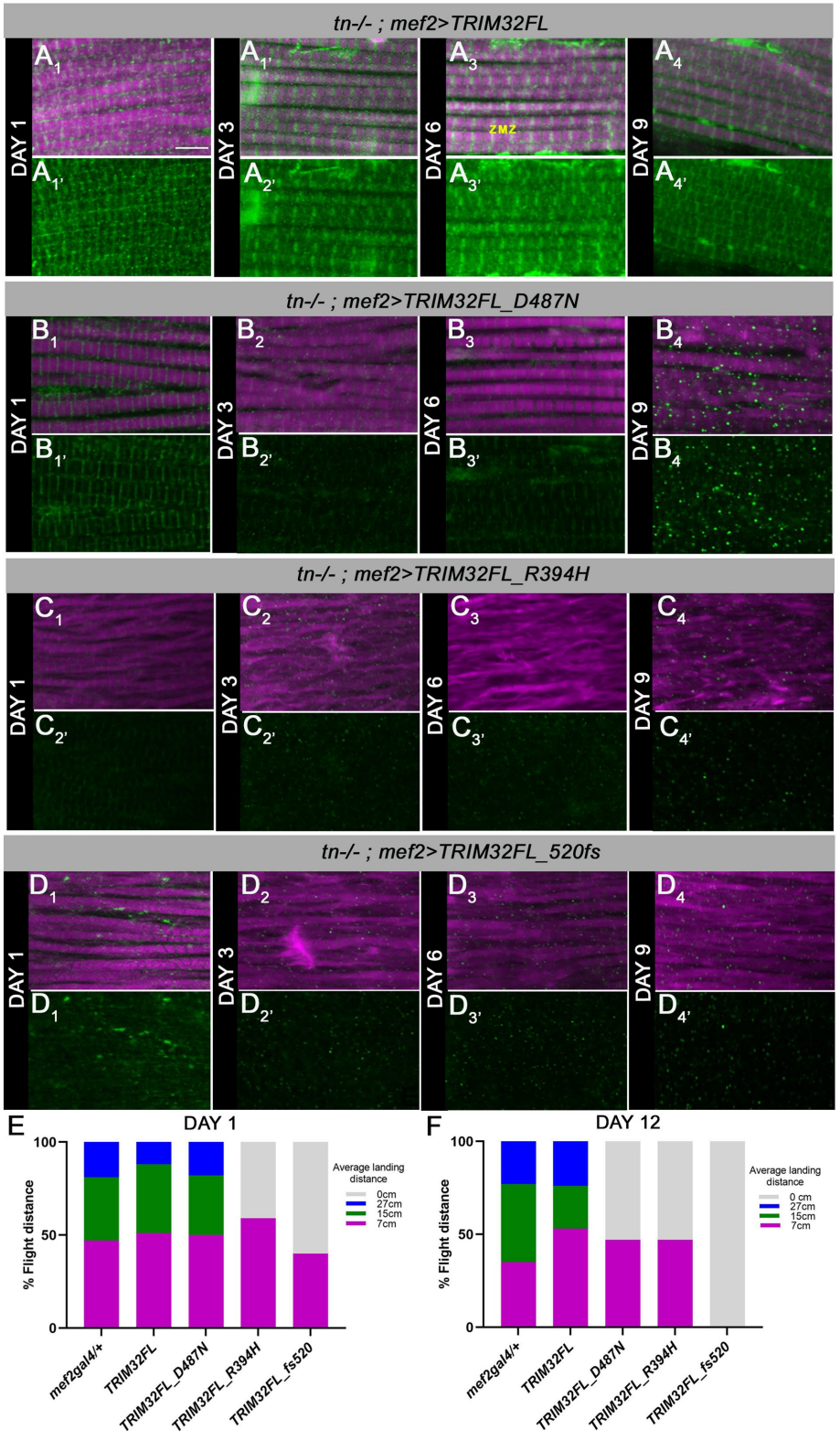

FIGURE 4: Human pathological mutations cause IFM defects and alter TRIM32 localization. IFMs labeled with phalloidin (magenta) and TRIM32 (green) to visualize myofiber architecture. (A_1–A_4) Overexpression of *TRIM32FL* in a *tn–/–* mutant background results in flies with normal adult flight muscles. TRIM32 is localized at the Z-disk and M-line within the myofibers at all timepoints examined. (B_1) Induction of the *D487N* mutation results in IFM's with *WT* morphology at day1. Myofibers show mild deterioration at day 3 (B_2) that continues to degenerate through day 6 (B_3) and day 9 (B_4). TRIM32 shows its normal sarcomere association at days 1–6, $B_{1'}$–$B_{3'}$. By day 9, $B_{4'}$, TRIM32 is no longer localized to sarcomeres, but appears in puncta. ($C_{1'}$–$D_{4'}$) In contrast, expression of the *R394H* and *520fs* mutations induced myofiber defects by day 1, C_1, D_1, that progressively worsened as the flies aged, C_2–D_4. In addition to myofibrillar anomalies, TRIM32 was not localized in the myofibers of *R394H*, $C_{1'}$–$C_{4'}$, or *520fs* mutants, $D_{1'}$–$D_{4'}$, and its expression appeared reduced compared with that of *TRIM32FL* control IFM. (E, F) Stacked bar graphs depicting flight ability of adult flies of the indicated genotypes in a *tn–/–* background at day 1, E, or day 12, F. Expression of all three mutations reduced flight ability. Scale bars: 10 µm, A_1–$D_{4'}$.

ability to fly long distances (~27 cm) at each time point (Figure 4, E and F). In contrast, *TRIM32* mutations showed reduced flight ability. The equivalent of the human *D487N* mutation exhibited normal flight at day 1, while 50% of these same flies lost their ability to traverse longer distances (>15 cm) by day 12. Consistent with IFM degeneration present by day 1, ~40–60% of flies expressing the *R394H* and *fs520* mutations were not able to fly. At day 12, this did not appreciably change for the *R394H* allele, while the *fs520* flies were flightless. Consistent with a progressive loss of myofibrillar organization, we also observed an age-dependent decrease in flight ability.

Structural changes associated with TRIM32 NHL domain mutations

Mutations may influence protein structure, stability, and/or dynamics, ultimately leading to protein dysfunction. The observed reduction, but not complete absence, of protein levels corresponding to TRIM32 mutants (Figure 3J) implies that these mutations allow partial protein function. To further assess the consequences of these mutations, we modeled the structural and energetic changes of the NHL domain associated with the *R394H* and *D487N* amino acid substitutions. To estimate the change in the Gibbs free energy of protein folding (ddG), calculations were performed using Rosetta's Cartesian ddG protocol (Park *et al.*, 2016) for the *Drosophila* TRIM32_NHL structure. The R394H-equivalent mutant was slightly more destabilizing than the D487N-equivalent mutant (+7.36 kcal/mol vs +7.20 kcal/mol). The resulting asparagine mutant in D487 was forced to present the hydrogen bond–donating nitrogen of the amide toward the other donator atoms in the side chains of R1208 and Q1210 (Supplemental Figure S5, A and A'). In contrast, the histidine that replaced the arginine in R394H/R1114 retained the positive charge, but due to its smaller size, it lost not only the

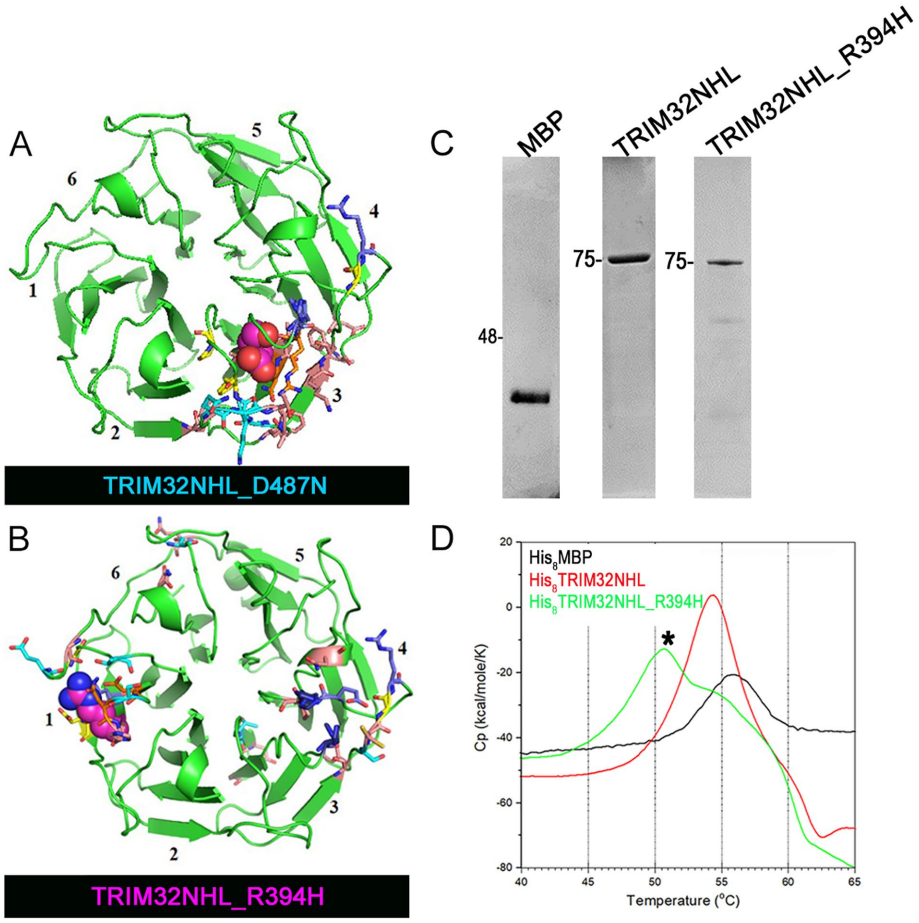

FIGURE 5: The R394H point mutation destabilizes the NHL structure. (A, B) The average energy of each residue in the top 100 lowest-energy members of each ensemble was calculated. The difference between the energies of the WT and D487N, A, or R394H, B, are shown. The site of mutation is shown in spheres. The mutated residues had at least a +2 REU increase in energy (magenta), while amino acids surrounding those residues have a small (0.2–0.4 REU) increase in energy (yellow), especially in D487N, A. Several other surrounding residues find lower-energy conformations of 0.2–0.4 REU (cyan), 0.4–1 REU (violet), or even 1–2 REU (dark blue), evident in NHL domain 4 of R394H, B. (C) Coomassie-stained nickel-column purified fractions of $His_{(8)}$MBP, $His_{(8)}$MBP _TRIM32NHL, and the $His_{(8)}$MBP_TRIM32NHL_R394H mutant protein. (D) Thermal unfolding transitions measured for $His_{(8)}$MBP (black), $His_{(8)}$MBP _TRIM32NHL (red), and $His_{(8)}$MBP _TRIM32NHL_R394H (green) using DSC.

salt bridge, but also a hydrogen bond network (Supplemental Figure S5, B and B′). Because the Cartesian ddG protocol sampling is limited to residues around the site of the mutation, we next used the relax protocol within Rosetta to generate an ensemble of structures to sample for differences in backbone conformations. Expectedly, there were perturbations in the backbone conformations around the sites of the mutations. For the D487N mutation in NHL3, most of the differences were in the vicinity of the mutation, while minor differences were observed in NHL 4 (Supplemental Figure S5C). Aside from the differences around the site of the R394H mutation in NHL1, several differences between the ensembles of backbone conformations were seen in repeats of NHL 3 and NHL 4 far from the site of the mutation (Supplemental Figure S5D).

Looking at the average per-residue energies within the ensembles, there is a trend to higher energies around the mutated residue. For example, D487N had a significantly higher energy than the original aspartic acid amino acid residue (–1.15 vs. –6.05 Rosetta energy units [REU], a full +4.90 difference). A number of the residues surrounding those in contact with D487N had a smaller increase in energy (0.2–0.4 REU), while most other surrounding residues found lower-energy conformations (Figure 5A). The R394H-equivalent mutant was different, in that the histidine mutant exhibited a more modest increase in energy over the original arginine residue (–1.77 vs. –4.16 REU, a difference of only +2.39 REU), while the residues finding higher or lower energies were spread around the entire protein, not just localized around the site of the mutation (Figure 5B). In fact, residues with higher and lower energies were seen in NHL repeats 3 and 4, where we observed the most changes in backbone conformation. These data, taken together, support our in vivo result that the R394H mutation is more destabilizing than D487N, possibly leading to structural changes that affect additional NHL repeats.

To confirm our modeling predictions using a biophysical approach, we utilized differential scanning calorimetry (DSC) to monitor changes in the thermal stability of TRIM32 mutants. Both WT (TRIM32NHL) and the TRIM32 point mutations (TRIM32NHL_R394H and TRIM32NHL_D487N) were fused to His_8MBP followed by a tobacco etch virus (TEV) cleavage site. In addition to MBP alone, we expressed and purified each of these fusion proteins, followed by incubation with TEV to remove the MBP tag. Unlike the TRIM32NHL protein, both mutant proteins were insoluble upon cleavage of the MBP tag, suggesting that the mutation affected the stability of the NHL domain. Hence, for thermal unfolding analysis, we chose to compare the TRIM32NHL and TRIM32 mutant proteins that retained the MBP fusion (Figure 5C). Purified MBP-TRIM32NHL_D487N was prone to aggregation and was not analyzed further. The heat capacity profile of MBP_TRIMNHL exhibited a single thermal transition with the midpoint temperature (T_m) around 54°C (Figure 5D, red trace). The observed signal is a superposition of the thermal unfolding of TRIM32NHL and the MBP domain, which by itself unfolds with T_m ~ 56°C (Figure 5D, black trace). Strikingly, the DSC thermogram for MBP_TRIM32NHL_R394H exhibited two distinct signals, a shoulder around 55°C that likely corresponded to the MBP domain and a major peak at 51°C (Figure 5D, green trace). A clear decrease in T_m for the thermal unfolding of TRIM32NHL induced by the R394H mutation provides evidence that the mutation renders the protein conformation less stable, providing a likely explanation for the observed decrease in TRIM32_R394H protein levels and muscle degeneration.

Tropomyosin protein levels are not altered in LGMD2H disease-causing alleles

Sarcomere maintenance requires a balance between protein synthesis and protein degradation. Thin filament–associated proteins,

such as tropomyosin (TM), troponin, and actin, undergo proteasomal degradation essential for preventing accumulation of damaged proteins (Carlisle *et al.*, 2017). Of the many muscle-specific targets, TM is a known mammalian substrate of TRIM32 (Cohen *et al.*, 2012). Furthermore, we recently showed that TRIM32 interacts physically with TM both in vitro and in vivo (Bawa *et al.*, 2020). These results prompted us to investigate whether TM expression and/or localization is altered upon loss of TRIM32 domains or in LGMD2H disease-causing alleles. We immunostained L3 larval muscles and examined the sarcomeric localization of TM. In *WT* (Supplemental Figure S6A) or *tn–/–; mef2>TRIM32FL* (Supplemental Figure S6D) control muscles, TM exhibited a normal sarcomeric distribution in the muscle. Consistent with our published results (LaBeau-DiMenna *et al.,* 2012), TM was mislocalized and abnormally accumulated within *tn–/–* myofibers (Supplemental Figure S6B). We observed similar results in muscles expressing the Δ*RING* (Supplemental Figure S6E) and Δ*NHL* (Supplemental Figure S6F) deletions of TRIM32, whereby TM predominantly accumulated along the degenerative myofibers with aberrant localization defects in the unbundled muscles. We further assessed the accumulation of TM in *tn–/–; mef2>TRIM32_ΔRING* and *tn–/–; mef2>TRIM32ΔNHL* by analyzing total protein levels in whole L3 larvae. Western blot analysis showed elevated levels of TM in *tn* mutants (Supplemental Figure S6C) or upon deletion of the RING domain (Supplemental Figure S6G) compared with *WT* (Supplemental Figure S6C) or *TRIM32FL*-rescued muscles (Supplemental Figure S6G). These data confirm that TM indeed is a substrate of *Drosophila* TRIM32 and the results further substantiate the functional conservation between human and fly TRIM32.

It was previously reported that TRIM32_D487N and R394H mutants lack the ability to ubiquitinate TRIM32 substrates (Locke *et al.*, 2009). Therefore, we wondered whether LGMD2H pathological mutations were also defective in regulating TM turnover. Upon immunostaining, we did not observe accumulation of TM in the myofibers of the *TRIM32 R394H, D487N*, or *520fs* alleles, and despite the presence of degenerative myofibers, TM was relatively well localized (Supplemental Figure S6, H–J). In addition, immunoblotting for TM showed no obvious changes in the overall protein levels of TM (Figure S6K). Taken together, our results provide evidence that TM undergoes normal ubiquitination and proteasomal degradation and is not implicated in disease progression, particularly with the investigated mutations.

TRIM32 pathological alleles cause elevated protein levels of costamere proteins

Integrins and sarcoglycans are core components of costamere complexes that link the actin cytoskeleton with the extracellular matrix and are crucial for the maintenance of the sarcolemma during muscle contraction (Anastasi *et al.*, 2008). We previously reported that βPS integrin (fly βPS is the vertebrate orthologue of the β1 subunit) distribution at the sarcolemma was perturbed upon loss of TRIM32 (LaBeau-DiMenna *et al.*, 2012). Consequently, we chose to investigate the correlation between point mutation–induced myofibrillar degeneration and disruption of the costameres in our LGMD2H model. *In vivo* staining of *WT* larval muscles with anti-βPS integrin revealed its normal association at the sarcolemma (Figure 6, A and A′). In contrast, βPS integrin distribution accumulated abnormally along the sarcolemma in TRIM32-deficient muscle (Figure 6, B and B′). Immunoblot analysis confirmed elevated βPS integrin protein levels in *tn* mutants (Figure 6C). We next examined βPS integrin localization and protein levels in TRIM32 disease-causing alleles, with *tn–/–; mef2>TRIM32FL* serving as a control for properly localized βPS integrin protein (Figure 6, D and D′). However, expression of the *R394H* mutation showed a separate, distinct staining pattern, whereby βPS integrin abnormally accumulated in the degenerative muscles and appeared diffused at the sarcolemma (Figure 6, E and E′). Small regions of βPS integrin showed an aberrant sarcolemmal distribution in *tn–/–; mef2>TRIM32_D487N* (Figure 6, F and F′) or *tn–/–; mef2>TRIM32_fs520* muscles (Figure 6, G and G′). Western blot analysis confirmed a strong trend towards increased βPS integrin protein levels in the disease-causing alleles as compared with *TRIM32FL* larvae (Figure 6H).

We previously reported that the in vivo localization of Scgδ, highly expressed in skeletal and cardiac muscle (Jung *et al.*, 1996), was perturbed upon loss of TRIM32 in larval muscles (LaBeau-DiMenna *et al.*, 2012). To examine this further, we analyzed the total protein levels of Scgδ. Interestingly, there was an ~50% increase in protein levels of Scgδ in *tn* mutants compared with *WT* (Figure 6I), suggesting that TRIM32 may regulate Scgδ protein levels through its E3 ligase activity. Because it is postulated that NHL repeats are essential for the recognition of TRIM32 substrates and that mutations in the NHL domain may disrupt protein–protein interactions, we also determined Scgδ protein levels in our pathological mutants. Immunoblot analysis confirmed up-regulation of Scgδ protein levels upon expression of the *R394H*, *D487N*, or *fs520* mutations (Figure 6J). Together, these data suggest that LGMD2H disease-causing mutations affect components of the costamere and the observed increase in protein levels likely contributes to disease progression.

To further confirm the evolutionary conservation of our results, we expressed GFP alone, GFP-tagged full-length TRIM32 (TRIM32FL), or a version lacking the RING domain (TRIM32_ΔRING) in murine C2C12 myoblasts and measured the relative levels of DGC components in immunoblot analyses. We found that expression of only the catalytically inactive TRIM32_ΔRING, but not GFP or TRIM32FL, resulted in increased α–dystroglycan, β–dystroglycans, and α–sarcoglycan accumulation (Figure 6, K and L). Overall, these data indicate that the E3 ligase activity of TRIM32 is required for degradation of costamere components in mammals as in flies.

DISCUSSION

It is unclear how loss of the single TRIM32 protein in muscle tissue initiates or promotes LGMD2H pathology. Interpretation of mouse TRIM32 models created to mimic LGMD2H pathology has proven complex, as both neurogenic and myopathic abnormalities are present in *TRIM32KO* or *TRIM32 D489N* knock-in mice (Kudryashova *et al.*, 2009, 2011). Moreover, loss of TRIM32 in satellite cells limits muscle regeneration (Kudryashova *et al.*, 2012; Nicklas *et al.*, 2012), thereby promoting further tissue deterioration. Here we took advantage of the lack of satellite cells in *Drosophila* larval muscles to separate the muscle-intrinsic function of TRIM32 from its role in mammalian muscle regeneration. We confirmed that a decrease in neuronal TRIM32 does not contribute to muscle pathology, while the expression of myopathic mutations in larval and adult muscle leads to pathogenic defects with reduced TRIM32 protein levels. Most importantly, we have substantiated a role for costameric proteins in disease progression.

Drosophila and human TRIM32 are evolutionarily conserved

TRIM32 is a multidomain protein that consists of RING domains and NHL repeats that are structurally and functionally conserved among different species. At least 12 different molecules, consisting of either RNA or protein, have been shown to interact with NHL-containing proteins (Tocchini and Ciosk, 2015). Moreover, mutations and/or deletions in the NHL region of TRIM family members are linked to

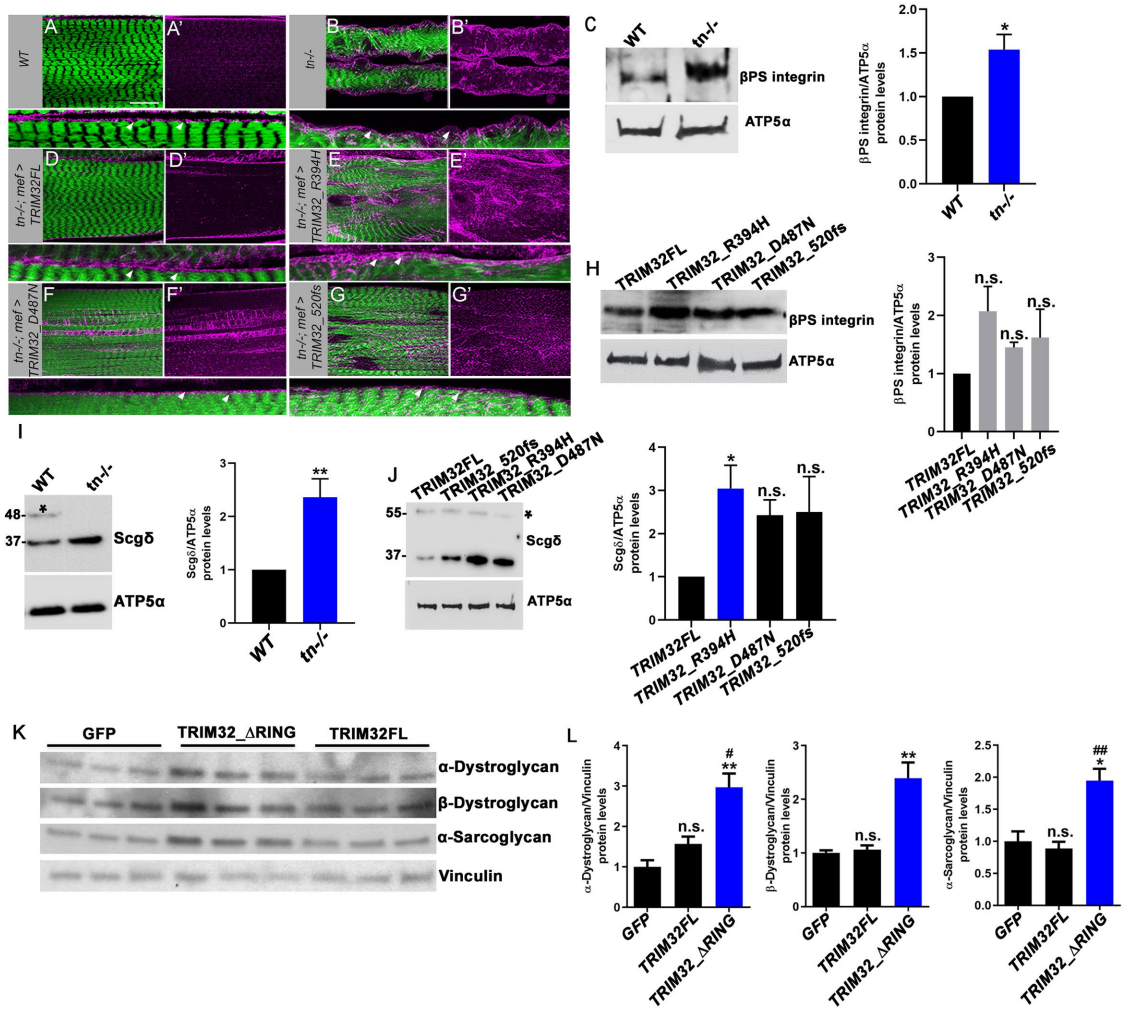

FIGURE 6: Costamere proteins accumulate abnormally upon loss of TRIM32 function in *Drosophila* or murine C2C12 cells. (A–B′, D–G) L3 larval muscles stained with phalloidin (green) and βPS integrin (magenta) to visualize muscle morphology. Horizontal panels are XZ confocal scans to show the sarcolemmal association of βPS integrin. (A, A′) βPS integrin localizes normally at the sarcolemma in *WT* larval muscle (white arrowheads). (B, B′) In *tn* mutants, βPS accumulates abnormally and appears diffuse at the sarcolemma (white arrowheads). (C) Immunoblot analysis of L3 whole larvae reveal elevated βPS integrin protein levels in *tn* mutants. Bar graph representing quantification of βPS-integrin/ATP5α protein levels. (D, D′) Muscle rescue with *TRIM32FL* reverts the βPS localization defect to *WT*. (E, E′) Transgenic expression of the *R394H* mutation causes βPS clustering at the sarcolemma (white arrowheads). (F, F′) βPS integrin is mostly normal at the sarcolemma, but increased along discrete regions, in *D487N* mutants. (G, G′) Abnormal distribution of βPS is prominent in degenerative myofibers in *520fs* mutants. (H) Increased βPS integrin protein levels are prominent in *R394H, D487N,* and *520fs* mutants expressed in a *tn–/–* background. Quantification of βPS-integrin/ATP5α protein levels represented by a bar graph. (I) Western blot depicts significantly high levels of Scgδ protein in *tn* mutants. Bar graph depicting the relative intensity of Scgδ/ATP5α. (J) Elevated Scgδ protein levels are prominent in all TRIM32 alleles expressed in a *tn–/–* background as compared with TRIM32FL control animals. Bar graph projecting Scgδ/ATP5α protein levels. (K) Total lysates from C2C12 myoblasts transfected for 48 h with the indicated plasmids were separated by SDS–PAGE. Immunoblotting was performed with antibodies against the indicated costamere protein components. Vinculin was used as loading control. (L) Bar graphs reporting an increase in α–dystroglycan, β–dystroglycan, and α–sarcoglycan protein levels upon expression of catalytically inactive TRIM32. $N = 3$, Mean ± SEM. **, $p < 0.01$; *, $p < 0.05$, n.s., nonsignificant. Scale bars: 10 μm.

diverse human diseases. In addition to LGMD2H caused by mutations in TRIM32, axonal neuropathy and gliomas result from mutations in TRIM2 and TRIM3, respectively (Boulay *et al.*, 2009; Ylikallio *et al.*, 2013). However, our understanding of how these repeats function in maintaining adequate protein–protein interactions, especially in muscle cytostructure, is limited.

Despite the moderate amino acid identity between *Drosophila* and human TRIM32, we demonstrate that structural homology of the entire NHL region is remarkably close and serves as an ideal model to investigate the downstream consequences of these myopathic mutations. Previous modeling of the R394H and D487N mutations used the crystal structure of the related NHL-containing protein *Drosophila* Brat (Saccone *et al.*, 2008) as a template. Our domain mutation analysis, based upon the structure we solved for TRIM32, reveals alterations that impact not only local protein structure. For example, the R394H mutation located in NHL domain 1

causes backbone perturbations and residue energy changes in NHL domains 3 and 4, thus providing a molecular understanding for the destabilization of the R394H mutant relative to WT NHL by DSC. These results provide evidence that mutations exert debilitating effects on NHL structure and reduce protein levels, further contributing to disease progression.

LGMD2H disease-causing mutations disrupt larval and adult musculature

Similar to LGMD2H patients, the expression of disease-causing alleles (*R394H, D487N* and *520fs*) in *Drosophila* larval muscle causes muscle degeneration with reduced TRIM32 protein levels and locomotor defects (Servián-Morilla *et al.*, 2019). Domsch *et al.* (2013) reported that RNAi-mediated knockdown of TRIM32 disrupts adult myofiber architecture at day 7 and day 11 after *tn RNAi* induction posteclosion. In contrast, our genetic assays show that expression of the *R394H* and *520fs* mutations in IFMs cause severe damage to the myofibers by day 1, which continue to degenerate with age. Expression of the *D487N* mutation also triggered muscle deterioration, but delayed compared with other mutations. It is also clear that TRIM32 protein levels correlate with protein destabilization and muscle degeneration. TRIM32 did not localize in the IFMs of *R394H* and *520fs* mutants, but remained relatively well localized in *D487N* mutant myofibers until day 3. In all destabilizing mutations, we observed variable accumulation of TRIM32 puncta. The presence of puncta, rather than the complete absence of protein, may indicate that TRIM32 no longer retains its correct sarcomeric association or possibly represents aggregated TRIM32 protein in response to the damage caused by the myopathic mutations. We believe that the differences in muscle degeneration and TRIM32 expression in different alleles partially explains the variable onset and phenotype severity observed in LGMD2H patients.

Do components of the DGC and integrin adhesion system play a critical role in LGMD2H disease progression?

Mutations in the DGC and integrin adhesion complex are associated with muscular dystrophies and cardiomyopathies (Straub *et al.*, 1997; Durbeej *et al.*, 1998; Durbeej and Campbell, 2002; Taverna *et al.*, 1998; Davies and Nowak, 2006; Jaka *et al.*, 2015). Deficiency of δ-sarcoglycan in mammalian skeletal muscle results in the absence of α-, β-, and γ-sarcoglycan, suggesting that sarcoglycan is a core component of sarcoglycan complex assembly (Hack *et al.*, 2000). Similarly, integrin adhesion molecules at the costamere are indispensable for the development and maintenance of sarcomeric architecture. Work performed in mice and flies showed that integrins play an important role in Z-disk formation (Volk *et al.*, 1990; Fässler *et al.*, 1996; Schwander *et al.*, 2003; Samarel, 2005; Sparrow and Schöck, 2009). Our previous work revealed that TRIM32 is essential for costamere integrity, whereby βPS integrin, talin, spectrin, vinculin, and Scgδ accumulate abnormally along the sarcolemma (LaBeau-DiMenna *et al.*, 2012). Our results here further support that loss of costamere stability may be involved in disease pathogenesis, as the expression of TRIM32 mutations also phenocopies the mislocalization of βPS integrin and Scgδ. Similar data were obtained upon expression of a catalytically inactive version of TRIM32 in murine myoblasts, extending in mammals the novel role of TRIM32 in promoting the degradation of *Drosophila* costamere components. Importantly, although TM protein is mislocalized upon loss of TRIM32, it retains its normal localization when pathogenic alleles are expressed in muscle tissue. These results suggest that TRIM32 can regulate the levels of sarcomeric proteins such as TM, but this accumulation is not sufficient to cause muscle degeneration as observed with costamere proteins.

Several studies have shown that upregulation of utrophin or integrin α7 partially compensates for the lack of dystrophin in *mdx* mice or in human DMD patients (Yucel *et al.*, 2018). Although the integrin adhesion complex (assayed by βPS integrin) and the DGC complex (assayed by Scgδ) are also up-regulated upon loss of TRIM32, this buildup of costameric proteins at the sarcolemma compromises the attachment between the membrane and myofibrils, leading to muscle degeneration. Some or all of these costamere proteins may be substrates for TRIM32 E3 ligase activity. The abnormal accumulation of βPS integrin and Scgδ along the sarcolemma may result from the inability to be ubiquitinated and turned over by the proteasome and/or the inability to maintain its normal localization due to protein damage during muscle contraction.

There are conflicting data about whether LGMD2H mutations in the NHL domain of TRIM32 inhibit multimer formation or alter ubiquitination activity (Lazzari and Meroni, 2016). We speculate that disease-causing mutations elevate protein levels of at least a subset of costamere proteins, either by altering protein interactions or by abolishing the catalytic activity of TRIM32. However, additional work is required to characterize the ubiquitination signature by TRIM32 and the resulting fate of substrate proteins. The structural and functional conservation of TRIM32, combined with the muscle-intrinsic *Drosophila* genetic model, will continue to provide novel insights into LGMD2H initiation and progression not currently available through study in other model organisms.

MATERIALS AND METHODS

Drosophila fly stocks

The following *Drosophila* stocks were obtained from the Bloomington (BL) *Drosophila* Stock Center (BDSC) or the Vienna *Drosophila* Resource Center (VDRC): *w*1118 was used as the *WT* control (BL3605); *mef2*-Gal4 (BL27390); *elav*-Gal4 (BL458); and UAS-*tn RNAi* (v19290). The *tnΔA* mutation was balanced over CyO, Tb/Sco (BL36335) balancer chromosome and non-Tb individuals were used for the *tn* mutant analysis (LaBeau-DiMenna *et al.*, 2012; Bawa *et al.*, 2020). *UAS-TRIM32FL* flies were described in LaBeau-DiMenna *et al.* (2012) and Bawa *et al.* (2020). All *UAS-TRIM32* deletion or point mutation fly lines were recombined into the *tnΔA* background for genetic analysis using standard techniques. All fly stocks were reared and maintained on standard cornmeal medium at 25°C unless otherwise indicated.

Generation of transgenic fly lines

UAS-TRIM32 deletion mutants. Clone GH06739 corresponding to full-length *tn_RA* was obtained from the *Drosophila* Genomics Resource Center (DGRC). Fragments corresponding to deletions missing the RING domain (TRIM32_ ΔRING) or the NHL domain (TRIM32_ΔNHL) were PCR amplified using the following primers:

TRIM32_ΔRING forward: 5′-AATAAGAATAGCGGCCGCATGAATCTGCGACGAGAGATCACG-3′

TRIM32_ΔRING reverse: 5′-CTAGTCTAGATCAGAAGACTTGGACGCGGTGATTC-3′

TRIM32_ΔNHL forward: 5′-AATAAGAATAGCGGCCGCATGGAGCAATTCGAGCAGCTGTTG-3′

TRIM32_ΔNHL reverse: 5′-CTAGTCTAGATCACTGCTGGCGCTTGCGCAGGTACACCTG-3′

Each amplified region was digested with NotI and XbaI restriction enzymes (RE site underlined) and subcloned into the pUAST *Drosophila* transformation vector. After sequence verification, all constructs were injected by Genetic Services to obtain transgenic flies.

UAS-TRIM32 human mutation alleles. UAST-TRIM32FL was used as a template to introduce the mutations using the QuikChange II XL Site-Directed Mutagenesis kit (Agilent Technologies). The following primer sequences were used:

TRIM32_R394H forward: 5′-CGACTCCAGCAACCACCACGTTCAGGTCTTCG-3′

TRIM32_R394H reverse –5′-CGAAGACCTGAACGTGGTGGTTGCTGGAGTCG-3′

TRIM32_D487N forward: 5′-GCTTCATTTACGTGTGCAATAAGGAGAACCACAGAGTGC-3′; TRIM32_D487N reverse: 5′-CACACGATTCGTGTTCGATCAGGCTATATAATGCGGATGCTC-3′ TRIM32_520fs forward: 5′-GAGCATCCGCATTATATAGCCTGATCGAACACGAATCGTGTG-3′ TRIM32_520fs reverse-5′-CACACGATTCGTGTTCGATCAGGCTATATAATGCGGATGCTC-3′

After sequence verification, all constructs were injected by Genetic Services for the creation of transgenic flies.

Immunostaining and microscopy

Wandering L3 larvae were heat-killed, filleted on SYLGARD plates in ice-cold 1X-PBS, and fixed using 4% formaldehyde (Fisher Scientific) at room temperature for 20 min (Bawa *et al.*, 2020). The fixed larvae were washed 3 times with PBS + 0.5% Tween 20 and the tissues were stained overnight at 4°C with the following primary antibodies: rat anti-TM (1:50; Babraham Institute); guinea pig anti-TRIM32 (1:100; LaBeau-DiMenna *et al.*, 2012); mouse anti-Lamin Dm_0/ADL67.10 (1:100; Developmental Studies Hybridoma Bank); and mouse anti-βPS integrin/CF.6G11 (1:50; Developmental Studies Hybridoma Bank). Post incubation with the primary antibodies, larval preps were washed with PBS + 0.5% Tween 20 and stained with the following fluorescent secondary antibodies: Alexa Fluor anti-rabbit 488, Alexa Flour anti-rat 594, and Alexa Flour anti-guinea pig 488 (1:400, Molecular Probes). Phalloidin 488 or Phalloidin 594 (1:400, Molecular Probes) was used to label F-actin. The stained tissues were mounted in anti-fade mounting medium (10% glycerol, 0.5% n-propyl gallate in 20 mM Tris buffer, pH 8.0). A Zeiss 700 confocal microscope was used to capture raw data. Image processing was performed using Photoshop.

Crystallization, data collection, and molecular modeling

Purified TRIM32_NHL (Bawa *et al.*, 2020) in 50 mM NaCl, 10 mM HEPES, pH 7.5 was concentrated to 9.4 mg/ml for crystallization screening. All crystallization experiments were setup using an NT8 drop-setting robot (Formulatrix) and UVXPO MRC (Molecular Dimensions) sitting drop vapor diffusion plates at 18°C. Protein (100 nL) and crystallization solution (100 nL) were dispensed and equilibrated against 50 µL of the latter. Prismatic crystals were obtained in 1–2 d from Index HT screen (Hampton Research) condition F7 (25% [wt/vol] PEG 3350, 100 mM Bis–Tris, pH 6.5, 200 mM ammonium sulfate). Samples were transferred to a fresh drop composed of 80% crystallization solution and 20% (vol/vol) PEG 200 and stored in liquid nitrogen. X-ray diffraction data were collected at the Advanced Photon Source beamline 17-ID using a Dectris Pilatus 6M pixel array detector.

Structure solution and refinement

Intensities were integrated using XDS (Kabsch, 1988, 2010) via Autoproc (Vonrhein *et al.*, 2011) and the Laue class analysis and data scaling were performed with Aimless (Evans, 2011). Structure solution was conducted by molecular replacement with Phaser (McCoy *et al.*, 2007) using a previously determined structure of Trim32 NHL (PDB 6D69) as the search model. The top solution was obtained in the space group $P2_12_12_1$ with a single molecule in the asymmetric unit. Structure refinement and manual model building were conducted with Phenix (Adams *et al.*, 2010) and Coot (Emsley *et al.*, 2010), respectively. Anisotropic atomic displacement parameters were refined for all atoms except water molecules. Disordered side chains were truncated to the point for which electron density could be observed. Structure validation was conducted with Molprobity (Chen *et al.*, 2010) and figures were prepared using the CCP4MG package (Potterton *et al.*, 2004). Structure superposition was conducted with GESAMT (Krissinel, 2012) via CCP4i (Winn *et al.*, 2011). The coordinates and structure factors for Trim32_NHL were deposited to the Worldwide Protein Databank (wwPDB) with the accession code 6XG7.

Human TRIM32 structure prediction

The structure of human TRIM32_NHL was computed by applying the following amino acid sequence to the I-TASSER (Zhang, 2008; Roy *et al.*, 2010) server (May 2020). The top model yielded a C-score of –0.14 and TM-score of 0.70 ± 0.12:

LKKMGAKGSTPGMFNLPVSLYVTSQGEVLVADRGNYRIQVFTRKGFLKEIRRSPSGIDSFVLSFLGADLPNLTPLSVAMNCQGLIGVTDSYDNSLKVYTLDGHCVACHRSQLSKPWGITALPSGQFVVTDVEGGKLWCFTVDRGSGVVKYSCLCSAVRPKFVTCDAEGTVYFTQGLGLNLENRQNEHHLEGGFSIGSVGPDGQLGRQISHFFSENEDFRCIAGMCVDARGDLIVADSSRKEILHFPKGGGYSVLIREGLTCPVGIALTPKGQLLVLDCWDHCIKIYSYHLRRYSTP

TRIM32 NHL domain mutation analysis

The structure of the NHL repeat region of *Drosophila* TRIM32 was prepared for ddG prediction by relaxing into cartesian space using coordinate restraints via Rosetta (Leaver-Fay *et al.*, 2011) and the lowest-energy structure was selected Rosetta's Cartesian ddG protocol (Park *et al.*, 2016). Briefly, the Cartesian ddG protocol ran for three iterations, and the energies were averaged among the three, with the predicted ddG being the difference between the *WT* and the mutant. For Rosetta relax computations to determine per-residue energies, the mutants were generated using Maestro, and point mutants, along with the *WT* protein were relaxed and minimized for 1000 independent trajectories. The 100 lowest-scoring structures were furthered for subsequent analysis.

βPS integrin antibody production

The peptide QSMRLALRVNEKHNC, corresponding to AAs 159-172 of *Drosophila* βPS integrin (FlyBase ID FBpp0071061), was conjugated to keyhole limpet hemocyanin (KLH) and injected into rabbits for antisera production. Antibodies specific for βPS integrin were affinity-purified using the antigen (Genscript).

Western blotting

Five to ten L3 larvae were homogenized in 4× Laemmli sample buffer (Bio-Rad). The resulting larval lysate was boiled at 100°C for 10 min and centrifuged at 15,000 rpm for 20 min to separate cellular debris. Lysate was stored at –20°C until further use. Lysates were subjected to SDS–PAGE to analyze overall protein levels, transferred to polyvinyl difluoride (PVDF) membranes (Pierce Biotechnology), and incubated with appropriate primary antibodies: guinea pig anti-TRIM32 (1:500; LaBeau-DiMenna *et al.*, 2012), rat anti-TM (1:500; Babraham Institute), rabbit anti-βPS integrin (1:1000; see description above), rabbit anti-Scgδ (1:500; LSBio), and mouse anti-ATP5α (1:10,000; Abcam) as a loading control. For the C2C12 experiments,

we used as primary antibodies mouse anti-α-dystroglycan (1:2000; Millipore), mouse anti-ß-dystroglycan (1:100; Hybridoma Bank), mouse anti-α-sarcoglycan (1:250; Monosan), and mouse anti-vinculin (1:5000; Sigma). To detect primary antibodies, horseradish peroxidase–conjugated secondary antibodies were used at a dilution of 1:5000 (GE Healthcare). Protein blots were developed using a Prometheus ProSignal Pico detection system (Genesee Scientific) and imaged using the FluorChem M system. For the C2C12 experiments, to detect primary antibodies, alkaline phosphatase (Promega)–conjugated secondary antibodies were used at a dilution of 1:7500. Protein blots were developed using CDP-star substrate (ThermoFisher Scientific) detection system and imaged using an Odyssey FC system. Densitometry analysis of protein levels was performed using ImageJ software.

Quantitative RT-PCR

Total RNA was isolated from a pool of three wandering L3 larvae using the RNAeasy Mini Kit (QIAGEN) for each genotype. After elution, RNA concentrations were determined and single-strand complementary DNA (cDNA) was generated from 300 ng of RNA using the qScript XLT cDNA SuperMix kit (Quanta Biosciences). For the qPCR reactions, each cDNA sample was diluted to 1:50 and mixed with Power UP SYBR Green Master mix and the appropriate primers (Applied Biosystems). *rp49* was used as the reference gene. The following primers were synthesized by Integrated DNA Technologies (IDT):

tn: 5′F-GAGCTGCATATCGAAATCACCG-3′; 5′R-AGATAGGCTTTTTCCGAGCAAAC-3′

rp49: 5′F-GCCCAAGGGTATCGACAACA-3′; 5R′-GCGCTTGTTCGATCCGTAAC-3′.

Three independent biological replicates were processed for each genotype and reactions were run in triplicate using the Quant Studio 3 Applied Biosystem with Quant studio design and analysis software. The average of the triplicates was used to calculate the $2^{-\Delta\Delta Ct}$ values (normalized fold expression).

Cell culture and transfection

C2C12 (ATCC), a myoblast cell line from the C3H mouse strain, was grown in DMEM (Dulbecco's modified Eagle's medium, Life Technologies), supplemented with FBS (Euroclone) and 2 mM L-glutamine, and maintained in culture at 37°C with 5% CO_2. The cells used were not contaminated by mycoplasma. C_2C_{12} myoblasts were transfected with plasmids expressing GFP, TRIM32FL-GFP, and TRIM32ΔRING-GFP (kindly provided by M. Kules-Martin, Oregon Health and Science University, Portland, OR) using Lipofectamine 2000 (ThermoFisher Scientific).

Phenotypic measurements and quantification

Muscle defect and diameter measurements. For muscle defect quantitation, muscles were characterized as defective if they exhibited morphology similar to that of *tn* mutant muscles, assessed by phalloidin staining (Figure 1, B, B′, and D). Percent defective muscles was calculated as the number of individual abnormal muscles divided by the total number of muscles. Each data point in the scatterplot represents the percentage of defective muscles per larva. At least 20 larvae were dissected for each genotype. The "Distance between two polylines" ImageJ plugin was used to measure the average diameter of each VL3 muscle. Raw values were imported into GraphPad Prism 8.0 for statistical analysis and graph generation. Each data point represents the average diameter for a single muscle.

Locomotion assay. Larval locomotion studies were performed as previously described (Brooks *et al.*, 2016).

Pupal axial ratio determination. Pupae of the indicated genotypes were removed from the vial and placed dorsal side up. Images were taken with a Leica M165 FC Stereomicroscope. Using ImageJ, the line and measure command were used for length and width measurements and the length/width ratios were calculated for each genotype ($N \geq 10$). These raw data were imported into Graphpad Prism 8.0 and plotted as a box and whiskers plot.

Internuclear distance measurements. To quantitatively measure the myonuclear distance in the LGMD2H disease-causing alleles, we analyzed the nuclei in VL3 larval muscles. Measurements were made using the segmented line tool in ImageJ. The shortest distance between the nuclei was reported and the internuclear distance between the nuclei that were clustered together was considered zero. Statistical analysis was performed using Graphpad Prism 8 software and each data point represents a single distance between two nuclei represented as a scatter plot.

Flight assay. One day after eclosion, individual flies of the indicated genotypes were anesthetized and placed into individual vials connected to a plexiglass flight chamber 17 cm (h) × 17 cm (w) × 27 cm (l). An illumination lamp was placed at the opposite end of the chamber. Flies were released from the vial after wakening and flight distance was recorded when the fly landed. Flies that showed normal takeoff flight behavior covered an average distance of 15 cm or 27 cm within the chamber. Flies that tried to fly, but ended up at the bottom of the chamber, traveled 7 cm. Flies that were unable to fly fell to the bottom of the chamber immediately and were scored as "no flight" with a distance of 0 cm. The same flies were collected and reanalyzed at day 12. Each recorded measurement was imported into Graphpad Prism 8 software for statistical analysis and represented as a bar graph based upon the percentage of flies who flew each distance. $N = 22$ flies for each genotype.

Statistical analysis

Statistical analysis was performed by automated software in Graphpad Prism 8.0 to prevent bias. Normally distributed data between two samples was analyzed using a two-tailed unpaired Student's *t* test. The Mann–Whitney U-test was used to compare two samples with nonparametric data. For multiple group comparisons, none of the data sets conformed to a Gaussian distribution and thus they were subjected to the Kruskal–Wallis test. Differences were considered significant if $p < 0.05$ and are indicated in each figure legend. A summary of all *n* values, statistical tests, and *p* values is detailed in Table S3.

Differential scanning calorimetry

The NHL region of *Drosophila* TRIM32 was PCR-amplified (nucleotides 3231-4062) from either *UAS-TRIM32* or *UAS-TRIM32_R394H* using the following primers:

MBP_NHL forward: 5′-TAACGCGTCGACAGTAGTAGCAGCAGCAGTGGCAGCAGCC-3′

MBP_NHL reverse: 5′-AATAAGAATGCGGCCGCTCAGAAGACTTGGACGCGGTGCTTC-3′

The amplified product was digested with SalI and NotI restriction enzymes (RE site underlined) and ligated into the digested pT7_MBP_HMT expression vector, a derivative of pT7HMT designed to express polyhistidine-tagged maltose-binding fusion

proteins cleavable by TEV protease (Geisbrecht *et al.*, 2006). Protein expression of the *Drosophila* TRIM32_NHL and TRIM32_NHL_R394H proteins were performed as described in Bawa *et al*. (2020). Purification was performed according to manufacturer protocol. To determine the thermal stability of the TRIM32NHL variants, purified protein (1 mg/ml) was dialyzed in PBS, degassed, and loaded into a VP-DSC MicroCalorimeter (MicroCalTM). The temperature was scanned at 1°C/min from 20 to 80°C. Heat capacity, *C*p (kcal/mol/K), was plotted after subtraction of a blank thermogram obtained without protein.

ACKNOWLEDGMENTS

We are grateful to the BDSC, VDRC, and DGRC for providing fly stocks or cDNAs essential for this project. Special thanks to Xin Xu for assisting with protein purification and to Brian V. Geisbrecht for providing the pT7_ MBP_HMT expression vector. This work was supported by funds from the National Institute of Arthritis and Musculoskeletal and Skin Disease (NIAMS) of the National Institutes of Health (NIH) under Awards R21AR073373 and 2R01AR060788 to E.R.G., R21AR066264 to S.E.A.B., and P20GM113117 to D.K.J. Funds for preliminary data were supported by the COBRE Center in Protein Structure and Function funded by the National Institute of General Medical Sciences of the NIH under Award P30 GM110761. S.B. was supported by a predoctoral fellowship through the American Heart Association (AHA), 19PRE34450211. Use of the IMCA-CAT beamline 17-ID at the Advanced Photon Source was supported by the companies of the Industrial Macromolecular Crystallography Association through a contract with Hauptman–Woodward Medical Research Institute. Use of the Advanced Photon Source was supported by the U.S. Department of Energy, Office of Science, Office of Basic Energy Sciences, under Contract DE-AC02-06CH11357.

REFERENCES

Adams PD, Afonine PV, Bunkoczi G, Chen VB, Davis IW, Echols N, Headd JJ, Hung LW, Kapral GJ, Grosse-Kunstleve RW, *et al.* (2010). PHENIX: a comprehensive Python-based system for macromolecular structure solution. Acta Crystallogr D Biol Crystallogr 66, 213–221.

Anastasi G, Cutroneo G, Santoro G, Arco A, Rizzo G, Bramanti P, Rinaldi C, Sidoti A, Amato A, Favaloro A (2008). Costameric proteins in human skeletal muscle during muscular inactivity. J Anat 213, 284–295.

Assereto S, Piccirillo R, Baratto S, Scudieri P, Fiorillo C, Massacesi M, Traverso M, Galietta LJ, Bruno C, Minetti C, *et al.* (2016). The ubiquitin ligase tripartite-motif-protein 32 is induced in Duchenne muscular dystrophy. Lab Invest 96, 862–871.

Barczyk M, Carracedo S, Gullberg D (2010). Integrins. Cell Tissue Res 339, 269–280.

Bawa S, Brooks DS, Neville KE, Tipping M, Sagar MA, Kollhoff JA, Chawla G, Geisbrecht BV, Tennessen JM, Eliceiri KW, *et al.* (2020). TRIM32 cooperates with glycolytic enzymes to promote cell growth. Elife 9.

Boppart MD, Mahmassani ZS (2019). Integrin signaling: linking mechanical stimulation to skeletal muscle hypertrophy. Am J Physiol Cell Physiol 317, C629–C641.

Borg K, Stucka R, Locke M, Melin E, Ahlberg G, Klutzny U, Hagen M, Huebner A, Lochmüller H, Wrogemann K, *et al.* (2009). Intragenic deletion of TRIM32 in compound heterozygotes with sarcotubular myopathy/LGMD2H. Hum Mutat 30, E831–E844.

Boulay JL, Stiefel U, Taylor E, Dolder B, Merlo A, Hirth F (2009). Loss of heterozygosity of TRIM3 in malignant gliomas. BMC Cancer 9, 71.

Brooks D, Naeem F, Stetsiv M, Goetting SC, Bawa S, Green N, Clark C, Bashirullah A, Geisbrecht ER (2020). *Drosophila* NUAK functions with Starvin/BAG3 in autophagic protein turnover. PLoS Genet 16, e1008700.

Brooks DS, Vishal K, Kawakami J, Bouyain S, Geisbrecht ER (2016). Optimization of wrMTrck to monitor *Drosophila* larval locomotor activity. J Insect Physiol 93–94, 11–17.

Campbell KP, Kahl SD (1989). Association of dystrophin and an integral membrane glycoprotein. Nature 338, 259–262.

Carlisle C, Prill K, Pilgrim D (2017). Chaperones and the proteasome system: regulating the construction and demolition of striated muscle. Int J Mol Sci 19.

Chen VB, Arendall WB 3rd, Headd JJ, Keedy DA, Immormino RM, Kapral GJ, Murray LW, Richardson JS, Richardson DC (2010). MolProbity: all-atom structure validation for macromolecular crystallography. Acta Crystallogr D Biol Crystallogr 66, 12–21.

Chiang AP, Beck JS, Yen HJ, Tayeh MK, Scheetz TE, Swiderski RE, Nishimura DY, Braun TA, Kim KY, Huang J, *et al.* (2006). Homozygosity mapping with SNP arrays identifies TRIM32, an E3 ubiquitin ligase, as a Bardet–Biedl syndrome gene (BBS11). Proc Natl Acad Sci USA 103, 6287–6292.

Ciechanover A (2006). The ubiquitin proteolytic system: from a vague idea, through basic mechanisms, and onto human diseases and drug targeting. Neurology 66, S7–S19.

Cohen S, Zhai B, Gygi SP, Goldberg AL (2012). Ubiquitylation by Trim32 causes coupled loss of desmin, Z-bands, and thin filaments in muscle atrophy. J Cell Biol 198, 575–589.

Cossée M, Lagier-Tourenne C, Seguela C, Mohr M, Leturcq F, Gundesli H, Chelly J, Tranchant C, Koenig M, Mandel JL, *et al.* (2009). Use of SNP array analysis to identify a novel TRIM32 mutation in limb-girdle muscular dystrophy type 2H. Neuromuscul Disord 19, 255–260.

Crosbie RH, Lebakken CS, Holt KH, Venzke DP, Straub V, Lee JC, Grady RM, Chamberlain JS, Sanes JR, Campbell KP (1999). Membrane targeting and stabilization of sarcospan is mediated by the sarcoglycan subcomplex. J Cell Biol 145, 153–165.

Davies KE, Nowak KJ (2006). Molecular mechanisms of muscular dystrophies: old and new players. Nat Rev Mol Cell Biol 7, 762–773.

Domsch K, Ezzeddine N, Nguyen HT (2013). Abba is an essential TRIM/RBCC protein to maintain the integrity of sarcomeric cytoarchitecture. J Cell Sci 126, 3314–3323.

Durbeej M, Campbell KP (2002). Muscular dystrophies involving the dystrophin–glycoprotein complex: an overview of current mouse models. Curr Opin Genet Dev 12, 349–361.

Durbeej M, Henry MD, Campbell KP (1998). Dystroglycan in development and disease. Curr Opin Cell Biol 10, 594–601.

Emsley P, Lohkamp B, Scott WG, Cowtan K (2010). Features and development of Coot. Acta Crystallogr D Biol Crystallogr 66, 486–501.

Ervasti JM, Ohlendieck K, Kahl SD, Gaver MG, Campbell KP (1990). Deficiency of a glycoprotein component of the dystrophin complex in dystrophic muscle. Nature 345, 315–319.

Evans PR (2011). An introduction to data reduction: space-group determination, scaling and intensity statistics. Acta Crystallogr D Biol Crystallogr 67, 282–292.

Fässler R, Georges-Labouesse E, Hirsch E (1996). Genetic analyses of integrin function in mice. Curr Opin Cell Biol 8, 641–646.

Fielitz J, Kim MS, Shelton JM, Latif S, Spencer JA, Glass DJ, Richardson JA, Bassel-Duby R, Olson EN (2007). Myosin accumulation and striated muscle myopathy result from the loss of muscle RING finger 1 and 3. J Clin Invest 117, 2486–2495.

Folker ES, Baylies MK (2013). Nuclear positioning in muscle development and disease. Front Physiol 4, 363.

Frosk P, Del Bigio MR, Wrogemann K, Greenberg CR (2005). Hutterite brothers both affected with two forms of limb girdle muscular dystrophy: LGMD2H and LGMD2I. Eur J Hum Genet 13, 978–982.

Frosk P, Weiler T, Nylen E, Sudha T, Greenberg CR, Morgan K, Fujiwara TM, Wrogemann K (2002). Limb-girdle muscular dystrophy type 2H associated with mutation in TRIM32, a putative E3-ubiquitin-ligase gene. Am J Hum Genet 70, 663–672.

Geisbrecht BV, Bouyain S, Pop M (2006). An optimized system for expression and purification of secreted bacterial proteins. Protein Expr Purif 46, 23–32.

Guglieri M, Straub V, Bushby K, Lochmüller H (2008). Limb-girdle muscular dystrophies. Curr Opin Neurol 21, 576–584.

Hack AA, Lam MY, Cordier L, Shoturma DI, Ly CT, Hadhazy MA, Hadhazy MR, Sweeney HL, McNally EM (2000). Differential requirement for individual sarcoglycans and dystrophin in the assembly and function of the dystrophin–glycoprotein complex. J Cell Sci 113 (Pt 14), 2535–2544.

Hayashi YK, Chou FL, Engvall E, Ogawa M, Matsuda C, Hirabayashi S, Yokochi K, Ziober BL, Kramer RH, Kaufman SJ, *et al.* (1998). Mutations in the integrin alpha7 gene cause congenital myopathy. Nat Genet 19, 94–97.

Henderson CA, Gomez CG, Novak SM, Mi-Mi L, Gregorio CC (2017). Overview of the muscle cytoskeleton. Compr Physiol 7, 891–944.

Hynes RO (2004). The emergence of integrins: a personal and historical perspective. Matrix Biol 23, 333–340.

Jaka O, Casas-Fraile L, López de Munain A, Sáenz A (2015). Costamere proteins and their involvement in myopathic processes. Expert Rev Mol Med 17, e12.

Jung D, Duclos F, Apostol B, Straub V, Lee JC, Allamand V, Venzke DP, Sunada Y, Moomaw CR, Leveille CJ, *et al.* (1996). Characterization of

delta-sarcoglycan, a novel component of the oligomeric sarcoglycan complex involved in limb-girdle muscular dystrophy. J Biol Chem 271, 32,321–32,329.
Kabsch W (1988). Automatic indexing of rotation diffraction patterns. J Appl Crystallogr 21, 67–72.
Kabsch W (2010). XDS. Acta Crystallogr D Biol Crystallogr 66, 125–132.
Krissinel E (2012). Enhanced fold recognition using efficient short fragment clustering. J Mol Biochem 1, 76–85.
Kudryashova E, Kramerova I, Spencer MJ (2012). Satellite cell senescence underlies myopathy in a mouse model of limb-girdle muscular dystrophy 2H. J Clin Invest 122, 1764–1776.
Kudryashova E, Struyk A, Mokhonova E, Cannon SC, Spencer MJ (2011). The common missense mutation D489N in TRIM32 causing limb girdle muscular dystrophy 2H leads to loss of the mutated protein in knock-in mice resulting in a Trim32-null phenotype. Hum Mol Genet 20, 3925–3932.
Kudryashova E, Wu J, Havton LA, Spencer MJ (2009). Deficiency of the E3 ubiquitin ligase TRIM32 in mice leads to a myopathy with a neurogenic component. Hum Mol Genet 18, 1353–1367.
LaBeau-DiMenna EM, Clark KA, Bauman KD, Parker DS, Cripps RM, Geisbrecht ER (2012). Thin, a Trim32 ortholog, is essential for myofibril stability and is required for the integrity of the costamere in *Drosophila*. Proceedings of the National Academy of Sciences of the United States of America 109, 17983–17988.
Lazzari E, Meroni G (2016). TRIM32 ubiquitin E3 ligase, one enzyme for several pathologies: From muscular dystrophy to tumours. Int J Biochem Cell Biol 79, 469–477.
Leaver-Fay A, Tyka M, Lewis SM, Lange OF, Thompson J, Jacak R, Kaufman K, Renfrew PD, Smith CA, Sheffler W, *et al*. (2011). ROSETTA3: an object-oriented software suite for the simulation and design of macromolecules. Methods Enzymol 487, 545–574.
Liu H, Niu A, Chen SE, Li YP (2011). Beta3-integrin mediates satellite cell differentiation in regenerating mouse muscle. FASEB J 25, 1914–1921.
Locke M, Tinsley CL, Benson MA, Blake DJ (2009). TRIM32 is an E3 ubiquitin ligase for dysbindin. Hum Mol Genet 18, 2344–2358.
Mahmood OA, Jiang XM (2014). Limb-girdle muscular dystrophies: where next after six decades from the first proposal (review). Mol Med Rep 9, 1515–1532.
McCoy AJ, Grosse-Kunstleve RW, Adams PD, Winn MD, Storoni LC, Read RJ (2007). *Phaser* crystallographic software. J Appl Cryst 40, 658–674.
Metzger MB, Pruneda JN, Klevit RE, Weissman AM (2014). RING-type E3 ligases: master manipulators of E2 ubiquitin-conjugating enzymes and ubiquitination. Biochim Biophys Acta 1843, 47–60.
Murphy AP, Straub V (2015). The classification, natural history and treatment of the limb girdle muscular dystrophies. J Neuromuscul Dis 2, S7–S19.
Nicklas S, Otto A, Wu X, Miller P, Stelzer S, Wen Y, Kuang S, Wrogemann K, Patel K, Ding H (2012). TRIM32 regulates skeletal muscle stem cell differentiation and is necessary for normal adult muscle regeneration. PLoS One 7, e30445.
Nigro V, Savarese M (2014). Genetic basis of limb-girdle muscular dystrophies: the 2014 update. Acta Myol 33, 1–12.
Park H, Bradley P, Greisen P, Liu Y, Mulligan VK, Kim DE, Baker D, DiMaio F (2016). Simultaneous optimization of biomolecular energy functions on features from small molecules and macromolecules. J Chem Theory Comput 12, 6201–6212.
Piccirillo R, Demontis F, Perrimon N, Goldberg AL (2014). Mechanisms of muscle growth and atrophy in mammals and *Drosophila*. Dev Dyn 243, 201–215.
Potterton L, McNicholas S, Krissinel E, Gruber J, Cowtan K, Emsley P, Murshudov GN, Cohen S, Perrakis A, Noble M (2004). Developments in the CCP4 molecular-graphics project. Acta Crystallogr D Biol Crystallogr 60, 2288–2294.
Roy A, Kucukural A, Zhang Y (2010). I-TASSER: a unified platform for automated protein structure and function prediction. Nat Protoc 5, 725–738.
Saccone V, Palmieri M, Passamano L, Piluso G, Meroni G, Politano L, Nigro V, (2008). Mutations that impair interaction properties of TRIM32 associated with limb-girdle muscular dystrophy 2H. Hum Mutat 29, 240–247.
Samarel AM (2005). Costameres, focal adhesions, and cardiomyocyte mechanotransduction. Am J Physiol Heart Circ Physiol 289, H2291–H2301.
Sardiello M, Cairo S, Fontanella B, Ballabio A, Meroni G (2008). Genomic analysis of the TRIM family reveals two groups of genes with distinct evolutionary properties. BMC Evol Biol 8, 225.
Schoser BG, Frosk P, Engel AG, Klutzny U, Lochmüller H, Wrogemann K (2005). Commonality of TRIM32 mutation in causing sarcotubular myopathy and LGMD2H. Ann Neurol 57, 591–595.
Schwander M, Leu M, Stumm M, Dorchies OM, Ruegg UT, Schittny J, Müller U (2003). Beta1 integrins regulate myoblast fusion and sarcomere assembly. Dev Cell 4, 673–685.
Servián-Morilla E, Cabrera-Serrano M, Rivas-Infante E, Carvajal A, Lamont PJ, Pelayo-Negro AL, Ravenscroft G, Junckerstorff R, Dyke JM, Fletcher S, *et al*. (2019). Altered myogenesis and premature senescence underlie human TRIM32-related myopathy. Acta Neuropathol Commun 7, 30.
Shokeir MH, Kobrinsky NL (1976). Autosomal recessive muscular dystrophy in Manitoba Hutterites. Clin Genet 9, 197–202.
Skinner BM, Johnson EE (2017). Nuclear morphologies: their diversity and functional relevance. Chromosoma 126, 195–212.
Slack FJ, Ruvkun G (1998). A novel repeat domain that is often associated with RING finger and B-box motifs. Trends Biochem Sci 23, 474–475.
Sparrow JC, Schöck F (2009). The initial steps of myofibril assembly: integrins pave the way. Nat Rev Mol Cell Biol 10, 293–298.
Straub V, Rafael JA, Chamberlain JS, Campbell KP (1997). Animal models for muscular dystrophy show different patterns of sarcolemmal disruption. J Cell Biol 139, 375–385.
Taverna D, Disatnik MH, Rayburn H, Bronson RT, Yang J, Rando TA, Hynes RO (1998). Dystrophic muscle in mice chimeric for expression of alpha5 integrin. J Cell Biol 143, 849–859.
Thrower JS, Hoffman L, Rechsteiner M, Pickart CM (2000). Recognition of the polyubiquitin proteolytic signal. EMBO J 19, 94–102.
Tocchini C, Ciosk R (2015). TRIM-NHL proteins in development and disease. Semin Cell Dev Biol 47–48, 52–59.
Vachon PH, Xu H, Liu L, Loechel F, Hayashi Y, Arahata K, Reed JC, Wewer UM, Engvall E (1997). Integrins (alpha7beta1) in muscle function and survival. Disrupted expression in merosin-deficient congenital muscular dystrophy. J Clin Invest 100, 1870–1881.
Volk T, Fessler LI, Fessler JH (1990). A role for integrin in the formation of sarcomeric cytoarchitecture. Cell 63, 525–536.
Vonrhein C, Flensburg C, Keller P, Sharff A, Smart O, Paciorek W, Womack T, Bricogne G (2011). Data processing and analysis with the autoPROC toolbox. Acta Crystallogr D Biol Crystallogr 67, 293–302.
Weissman AM (2001). Themes and variations on ubiquitylation. Nat Rev Mol Cell Biol 2, 169–178.
Winn MD, Ballard CC, Cowta KD, Dodson EJ, Emsley P, Evans PR, Keegan RM, Krissinel EB, Leslie AG, McCoy A, *et al*. (2011). Overview of the CCP4 suite and current developments. Acta Crystallogr D Biol Crystallogr 67, 235–242.
Ylikallio E, Pöyhönen R, Zimon M, De Vriendt E, Hilander T, Paetau A, Jordanova A, Lönnqvist T, Tyynismaa H (2013). Deficiency of the E3 ubiquitin ligase TRIM2 in early-onset axonal neuropathy. Hum Mol Genet 22, 2975–2983.
Yucel N, Chang AC, Day JW, Rosenthal N, Blau HM (2018). Humanizing the mdx mouse model of DMD: the long and the short of it. NPJ Regen Med 3, 4.
Zhang Y (2008). I-TASSER server for protein 3D structure prediction. BMC Bioinformatics 9, 40.